vibration

MDPI

Article

Active Vibration Control Performance Comparison Based on Middle Pedestal Stiffness Using a Mobility Model and the Narrowband Fx-LMS Technique

Anmok Jeong [1,*], Kyuchul Jung [2], Youngcheol Park [3], Junyeong Heo [3] and Hakjun Lee [1,*]

[1] Korean Institute of Industrial Technology, Cheonan 31056, Republic of Korea
[2] RMS Technology Co., Ltd., Cheonan 31217, Republic of Korea
[3] Division of Software, Yonsei University, Wonju 26493, Republic of Korea
* Correspondence: amjeong@kitech.re.kr (A.J.); hak1414@kitech.re.kr (H.L.)

Abstract: Vibrations generated from equipment mounted on ships radiate into the water and affect covert operation capabilities. Accordingly, various studies are being conducted to reduce vibration transmitted from mounted equipment. In this study, a system consisting of mounting equipment, a 3-axis active mount, a middle pedestal, and a lower mount of the middle pedestal was modeled using a finite element analysis program, and a mobility model was constructed by calculating the frequency response function between the positions required for analysis. The error signal (primary path) obtained using the mobility model and the response at the operating point by the control force of the actuator (secondary path) are applied to the narrowband Fx-LMS algorithm for vibration control, and the control performance was compared. Through coupling analysis of the middle pedestal, the control influence according to the rigidity of the middle pedestal was analyzed. As a result of the control simulation, the time required for vibration control was controlled approximately 6 times faster in the model, with increased stiffness of the middle pedestal, and the vibration reduction performance was predicted to improve by a minimum of 0.9 dB and a maximum of 13.3 dB. Through this study, a simulation model that can provide a guide for the design of the middle pedestal of a ship was obtained, and it is expected that it can be utilized for a preliminary design review before manufacturing the middle pedestal of a ship.

Keywords: mobility model; vibration reduction; finite element analysis; active vibration control; Fx-LMS; active mount

Citation: Jeong, A.; Jung, K.; Park, Y.; Heo, J.; Lee, H. Active Vibration Control Performance Comparison Based on Middle Pedestal Stiffness Using a Mobility Model and the Narrowband Fx-LMS Technique. *Vibration* **2024**, *7*, 999–1012. https://doi.org/10.3390/vibration7040053

Academic Editor: Lorenzo Dozio

Received: 19 September 2024
Revised: 14 October 2024
Accepted: 18 October 2024
Published: 29 October 2024

1. Introduction

Equipment mounted on naval ships generates vibrations while the ship is in operation, and the structural transmission sound generated by the vibration of the equipment is transmitted externally through the ship's body and radiated into the water. This is especially important for warships, as such noise can inform the enemy of their location and degrade the performance of underwater target detection systems using sonar. Reducing noise radiated into the water is essential to enhance stealth capabilities and ensure crew survivability. To address this, ship systems require high-performance mounts, and research is being conducted in various directions in the industry to reduce vibrations transmitted from above [1–8]. Previously, methods for reducing vibration using materials such as rubber mounts [9] were common, and studies were mainly conducted to reduce vibration by improving the characteristics of elastic mounts, which are the paths for structural vibration transmitted from the upper part. However, using only elastic mounts may be structurally simple and effective within a certain frequency range, but has limitations in resolving low-frequency and horizontal vibrations corresponding to the structural vibration frequency of the system. Recently, studies have been conducted to control vibration by applying control force using hybrid mounts that combine electromagnetic actuators and

piezoelectric stack actuators [10–13]. In the process of controlling vibration using such active mounts, a control algorithm for effective vibration control is required. The PID (proportional–integral–derivative) control method [14–16] is relatively simple and provides stable performance, but it requires prior knowledge of the dynamic characteristics of the target system, is difficult to configure control for multiple channels, and has difficulty responding quickly to complex vibration patterns. To solve these problems, the Fx-LMS (Filtered-x Least Mean Squares) [17–21] method has been introduced, and among them, research on the narrowband Fx-LMS algorithm is increasing. The narrowband Fx-LMS algorithm can effectively control vibration by filtering the input signal in real time and adjusting the output signal. In this study, a vibration reduction test device similar to the operational state of a ship was modeled using a finite element analysis program, and a mobility model was constructed by calculating the frequency response function between the positions required for the analysis. The primary and secondary paths required for active vibration control simulation were obtained using the finite element analysis program, and each path was applied to the narrowband Fx-LMS algorithm for vibration control, and the control performance according to the stiffness size of the middle pedestal was predicted and compared when the exciting force occurs from the upper-mounted equipment. In the existing vibration reduction technology using elastic mounts, research results have been published that the greater the stiffness of the middle pedestal, the greater the vibration reduction effect. However, in the case of a system combining an elastic mount and an actuator, most of the research on vibration reduction performance according to the stiffness of the middle pedestal is related to defense technology, so specific information has not been disclosed. In general, in vibration control using an actuator, the size of the signal input to the sensor is large, so control can be easy. On the other hand, in the case of small micro-vibrations transmitted through an elastic mount, it is difficult for the sensor to detect them sensitively, so control can become complicated. Therefore, information on under what conditions the middle pedestal can effectively control vibration is limited. Therefore, this study aims to predict the vibration control characteristics according to the stiffness of the middle pedestal through simulation. To this end, two models were considered. The first model is Case 1 (Young's modulus: 2×10^{11}), which uses the material properties of an actual production model, and the second model is Case 2 (Young's modulus: 2×10^{13}), which increases Young's modulus by 100 times to be similar to the floor foundation impedance of an actual naval ship. Vibration control simulations were performed targeting the fundamental frequency and the second and third harmonic frequencies of 60 Hz, 120 Hz, and 180 Hz, which correspond to the equipment operating speed (typically about 3600 rpm).

2. Materials and Methods

2.1. Ship Vibration Reduction Test Equipment

The vibration reduction test device is an experimental device that simulates an environment similar to a real ship. The vibration reduction test device is a device that is equipped with six three-axis active mounts and installs a device on the top of the structure to simulate the vibration of the mounted equipment, thereby enabling active vibration control experiments. The configuration of the vibration reduction test device is shown in Figure 1. It consists of a mounted device to simulate the vibration of the equipment mounted on the ship, a middle pedestal assuming the ship's raft, a passive mount under the middle pedestal, a three-axis active mount for vibration control, and an air mount for vibration isolation from the floor.

- Onboard equipment: Equipment that generates vibrations similar to those of equipment actually installed on a ship.
- Middle pedestal: This structure simulates the raft of the ship, with passive mounts installed underneath.
- Three-axis active mount: Installed under the mounted equipment to pedestal it and reduce the vibration transmitted from the equipment. This assembly is composed of three actuators to control vibrations in the x, y, and z directions (refer to Figure 2).

- Air mounts: These are used for vibration isolation from the floor.

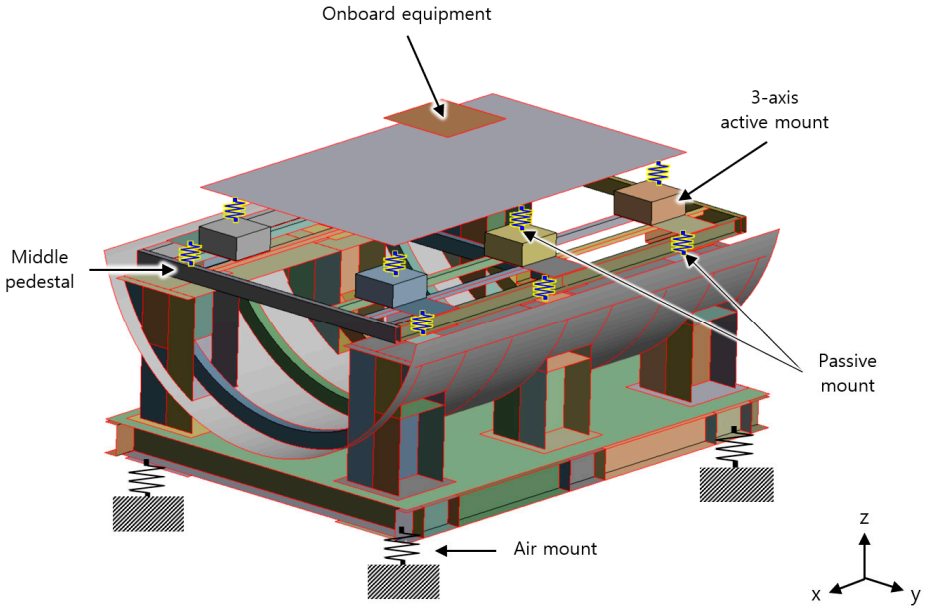

Figure 1. Ship vibration reduction test equipment.

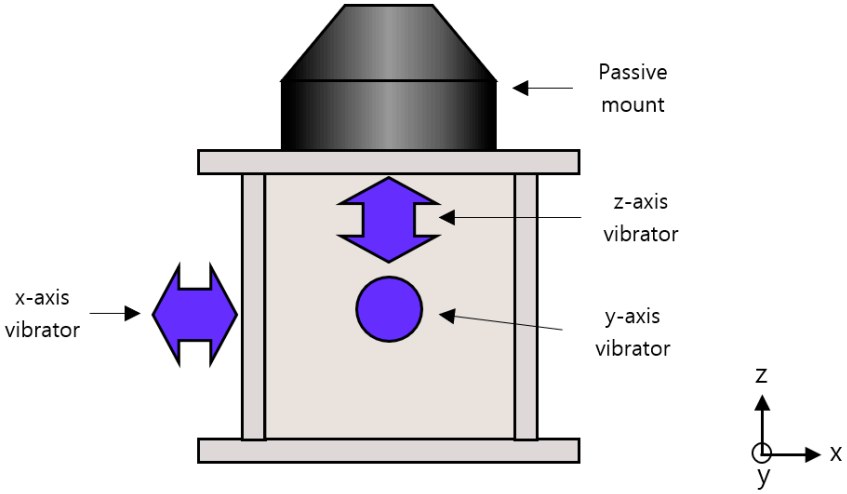

Figure 2. 3-axis active mount configuration (front view).

The vibration reduction mechanism works by applying electromagnetic control forces of the same frequency and amplitude and the opposite phase to the vibrations generated by the mounted equipment. This reduces the vibrations transmitted to the middle pedestal and the ship's hull (refer to Figure 3). The actuators attached to the 3-axis active mount are of the inertial type using electromagnetic forces. They generate inertial forces through the moving mass inside the actuators and apply these forces to the structure to reduce vibrations. With this design, the vibration reduction test equipment provides an effective environment for evaluating the vibration reduction performance under various vibration conditions.

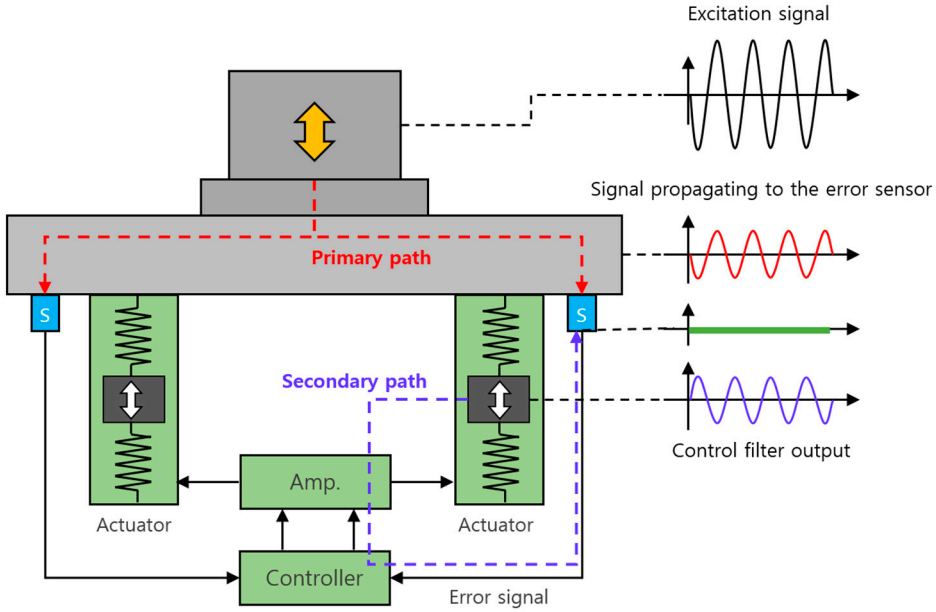

Figure 3. Mechanism for vibration reduction.

2.2. Mobility Model Using Finite Element Analysis

A finite element analysis model was used to calculate the mobility of the vibration reduction test device. Mobility, a type of frequency response function, is the inverse of mechanical impedance and is defined as the ratio of the velocity at a specific location to the force applied at the same or different location. It describes the relationship between force and velocity response and is used to analyze the dynamic characteristics of the system. Mobility can be expressed as follows:

$$M = V/F \tag{1}$$

where

M: Mobility (m/s/N);

F: Force applied to the structure (N);

V: Response velocity (m/s).

The finite element analysis was conducted using shell elements, and the boundary conditions for the analysis are illustrated in Figure 4. The passive mounts (K_1, K_2) and the air mount (K_3) were modeled using bushing joint components to examine the dynamic characteristics in the x, y, and z directions. The bushing joint component is a joint element capable of defining the dynamic stiffness in both vertical and horizontal directions, allowing the dynamic stiffness to be applied to the FEA model through displacement as a function of force. The specifications of the vibration reduction test device and the parameters for the finite element analysis are presented in Table 1. The weight of the mounted equipment is approximately 45% of the total weight of the test device. The passive mounts (K_1, K_2) are products from W Company, and to ensure that the dynamic characteristics are similar to those of the actual system, the dynamic stiffness was applied based on the data sheet from the product catalog. The stiffness of the air mount (K_3) was set to a value that achieves a system resonance frequency of 2 Hz.

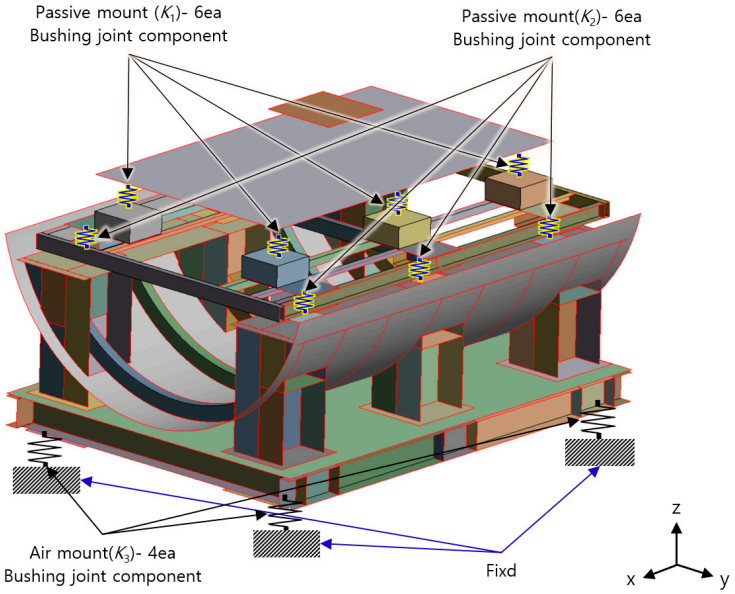

Figure 4. FEM modeling and boundary condition.

Table 1. Ship vibration reduction test equipment spec.

Onboard Equipment Weight (kg)	45% of the Total System Weight
Passive mount stiffness (N/m)	K_1: Data sheets of the products used K_2: Data sheets of the products used K_3: Stiffness for a resonance frequency of 2 Hz in the system

2.3. Active Vibration Control Simulation Method for Ship Vibration Reduction Test Equipment

In this study, we compared the control performance based on the stiffness of the middle pedestal when the excitation force is applied to the mounted equipment using an adaptive algorithm called Filtered-x Least Mean Squares (Fx-LMS). Figure 5 is a block diagram of a typical active vibration control system using an adaptive algorithm. The area indicated by the blue dotted line in this figure means the actual system coupled with the equipment that generates vibration, where $u(n)$ represents the input signal, $y(n)$ represents the output signal, and $e(n)$ represents the error signal. This algorithm works with the goal of updating the coefficients $w(n)$ of the control filter to reduce the error signal and converge the error signal to '0'. This algorithm is a method of applying the LMS adaptive formula after filtering the reference signal with the second-path impulse response to prevent the optimal solution of the adaptive filter from being distorted by the path between the filter output and the error sensor. When using the N-order FIR adaptive filter, the coefficient update formula is as follows.

$$\boldsymbol{w_i(n+1) = w_i(n) + \mu r(n-i)e(n), i = 0, 1, \ldots, N-1} \tag{2}$$

In the above equation, $r(x)$ is the following filtered reference signal.

$$\boldsymbol{r(n) = x(n) \otimes s_n = \sum_{i=0}^{L-1} s_{n,i} x(n-i)} \tag{3}$$

This signal is the signal filtered by the secondary path impulse response $s_{n,i}, i = 0, 1, \ldots L-1$ of the reference input signal $x(n)$ and L is the order of the filter modeling the secondary path. The control simulation method for the vibration reduction test device is depicted in Figure 6. As previously described, mobility was calculated using a finite element analysis program, and the primary and secondary paths necessary for vi-

bration control simulation were obtained. Each path obtained using finite element analysis was applied to the Fx-LMS control algorithm, and control performance according to the stiffness of the middle pedestal was compared through a simulation.

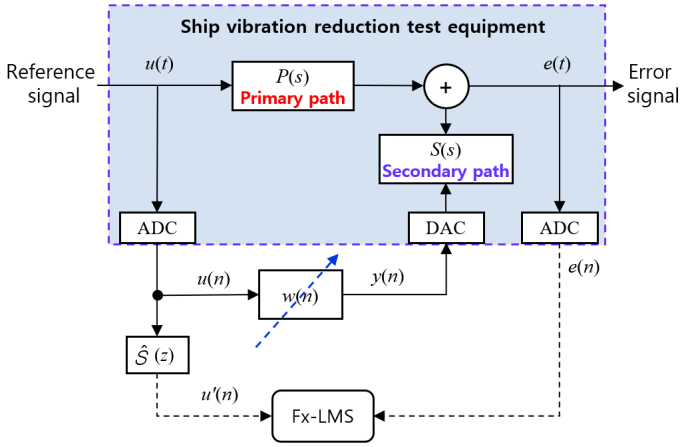

Figure 5. Block diagram of Fx-LMS.

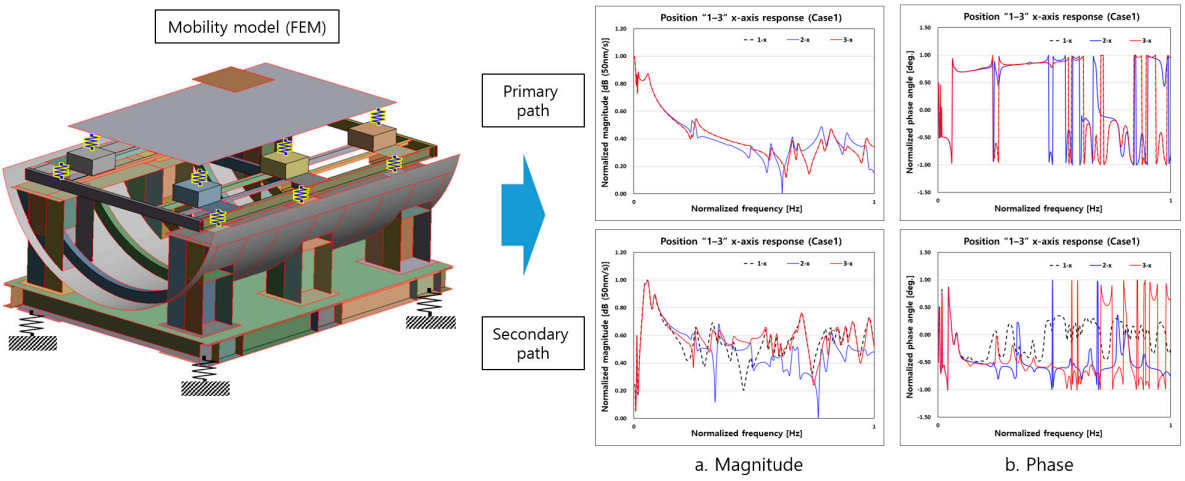

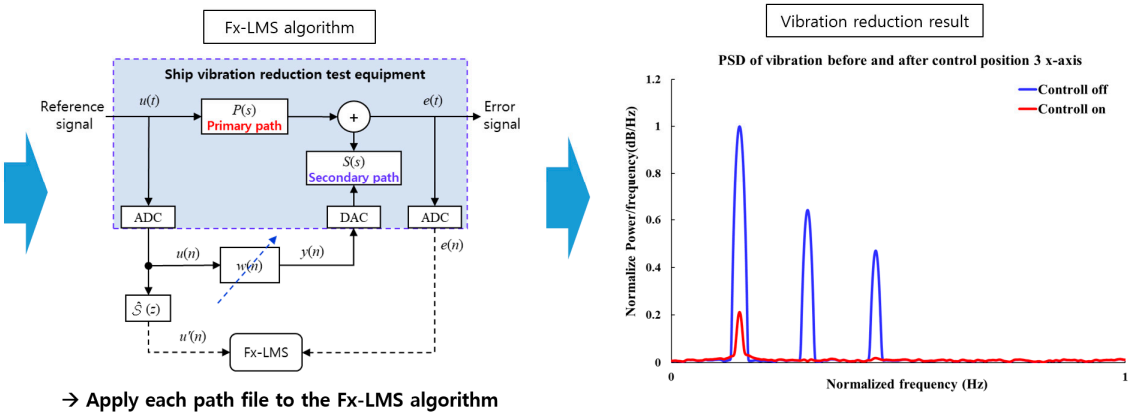

Figure 6. Vibration control simulation process for ship vibration reduction test equipment.

2.3.1. Primary Path

In this study, the primary path and secondary path required for vibration control simulation were acquired using a mobility model created through a finite element analysis

program. The primary path is the route through which vibrations generated by the upper-mounted equipment reach the error sensor, and it represents the response characteristics that propagate from the vibration source to the control target location. As shown in Figure 7, the primary path was determined by exciting the noise source of the mounted equipment in the x, y, and z directions with an excitation force corresponding to 70 dB (velocity, ref. 5×10^{-8} m/s). The frequency responses in the x, y, and z directions at positions 1 to 6 of the active mount, where the error sensors are attached, were obtained through frequency response functions.

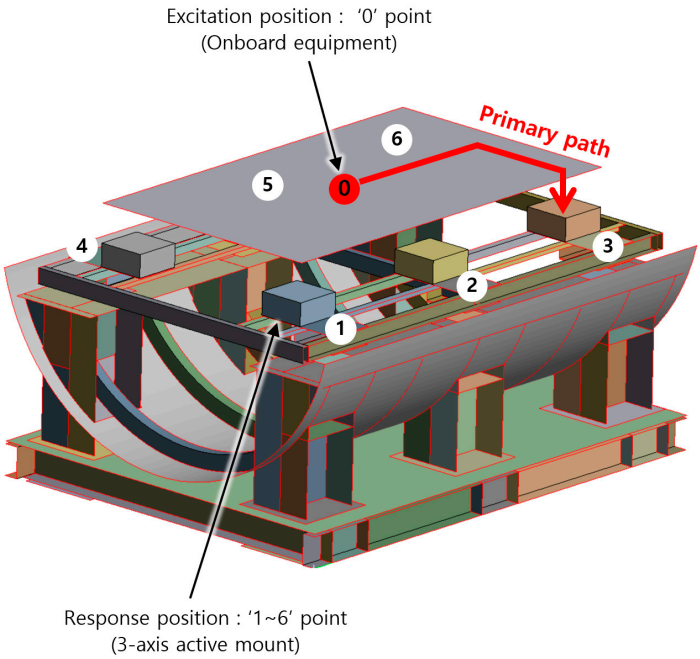

Figure 7. Excitation point and response point for primary path signal acquisition.

2.3.2. Secondary Path

The secondary path is the path through which the output of the control filter reaches the error sensor, and represents the response characteristics transmitted to the controlled target position by the vibration control force of the actuator when the actuator operates for vibration control. The input of the secondary path is the control force of the actuator, and the output is the vibration response at the controlled position, which includes the dynamic characteristics of the power amplifier, the actuator, and the controlled target structure. Figure 8 shows the method for obtaining a secondary path. The secondary path was excited in the x, y, and z directions, respectively, at the active mount position where the actuator was attached, and the response characteristics were obtained as a frequency response function in the same way at the active mount 1 to 6 positions, which are the control force operating points. The operating force and phase dynamic characteristics of the actuator applied to the system were reflected when obtaining the secondary path using finite element analysis, which enabled the vibration control characteristics by the exciting force of the actual system to be reflected. The dynamic characteristics of the actuator for control are shown in Figure 9. The actuator used to apply the control force has a natural frequency of less than 20 Hz and is designed to have a characteristic of maximum force at a frequency three times the natural frequency. The actuator has a characteristic of force linearity within $\pm 10\%$ in the target frequency range.

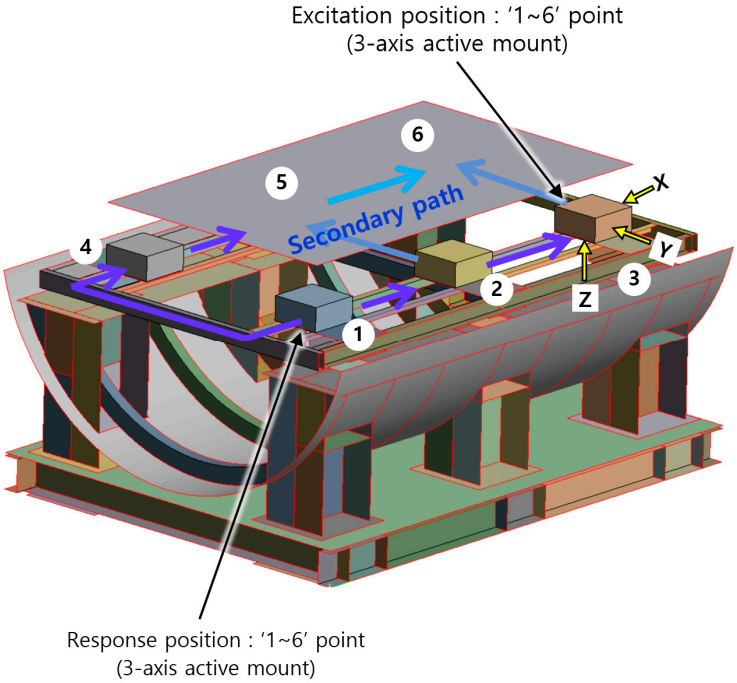

Figure 8. Excitation point and response point for secondary path signal acquisition.

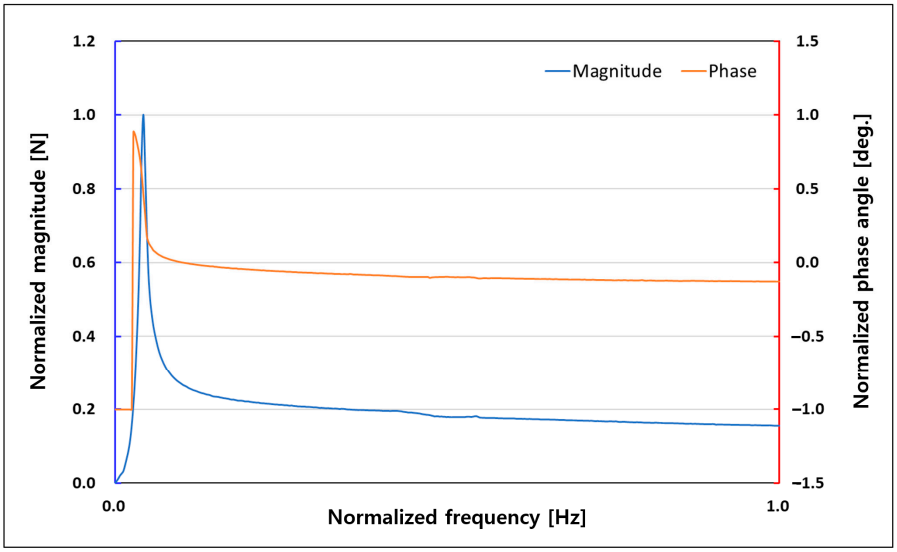

Figure 9. Characteristic curve of inertial actuator.

3. Results

3.1. Review of Coupling of the System According to the Stiffness of the Middle Pedestal

To compare the control performance according to the stiffness of the middle pedestal, the vibration mode coupling of the middle pedestal was analyzed. The mode coupling of the middle pedestal refers to the response characteristics at the locations of adjacent 3-axis active mounts when the actuators of the 3-axis active mounts apply control forces to control the transmitted vibration. As shown in Figure 10, an exciting force was applied to one 3-axis active mount using the dynamic characteristics of the actuator, and the responses were obtained from adjacent 3-axis active mount assemblies. Since the vibration reduction test equipment has a symmetrical shape, this study applied excitation forces to the 3-axis active mount at position 1 along the x, y, and z axes, respectively, and observed the responses generated from the 3-axis active mount assemblies at positions 2 and 3. The actual response

characteristics at positions 4, 5, and 6 were examined and found to be identical to the responses of the 3-axis active mounts at positions 1, 2, and 3.

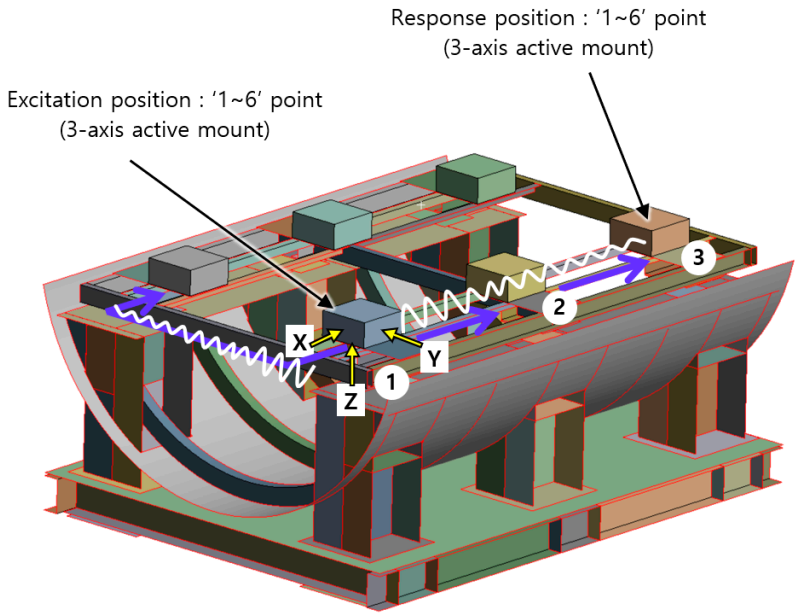

Figure 10. Excitation and response position for coupling analysis of middle pedestal.

Figure 11 shows the response characteristics in the x, y, and z directions of the 3-axis active mount at adjacent control locations 1, 2, and 3 when an excitation force is applied to the 3-axis active mount at location 1 in the horizontal (x-axis) direction, with the x- and y-axes normalized. In the figure, the black dotted line represents the response from the excited location to the excited direction, the blue solid line represents the response characteristics at location 2, and the red solid line represents the response characteristics at location 3. The upper figure of Figure 11 represents the response characteristics in a log scale, and, in the case of the lower figure, the difference between the maximum and minimum values of the response is large, making it difficult to read this figure, so the normalized Y-axis is shown as 0.4. As shown in this figure, even when an excitation force is applied to the 3-axis active mount at position 1 in the horizontal (x-axis) direction, there is a frequency range where a larger response occurs than the 3-axis active mount at other control positions. Specifically, compared to the locations where the excitation force was applied, it is predicted that larger responses will occur in the x-direction (103 Hz) and z-direction (56 Hz) at location 2, and in the y-direction (96 Hz, 131 Hz) at locations 1 and 3.

Figure 12 shows the response characteristics in the x, y, and z directions of the 3-axis active mount at adjacent control positions 1, 2, and 3 when an excitation force is applied to the 3-axis active mount at position 1 in the vertical (z-axis) direction, with the x- and y-axes normalized. In the figure, the black dotted line represents the response from the excited position to the excited direction, the blue solid line represents the response characteristic at position 2, and the red solid line represents the response characteristic at position 3. The upper figure of Figure 12 represents the response characteristics in a log scale, and in the case of the lower figure, the difference between the maximum and minimum values of the response is large, making it difficult to read this figure, so the normalized Y-axis is represented as 0.4. As can be seen in this figure, even if the excitation is applied at position 1 in the vertical (z) direction, there is a frequency range where a larger response occurs in the 3-axis active mount of other control positions. Specifically, compared to the locations where the excitation force was applied, a larger response is predicted to occur at location 2 in the x direction (141 Hz), and at locations 1 and 3 in the y direction (76 Hz, 131 Hz). As can be seen from the modal analysis results in the figure, this is attributed to the structural mode of

the middle pedestal. The response characteristic graphs indicate significant vibration mode coupling between adjacent 3-axis active mounts for control, resulting in highly complex response characteristics.

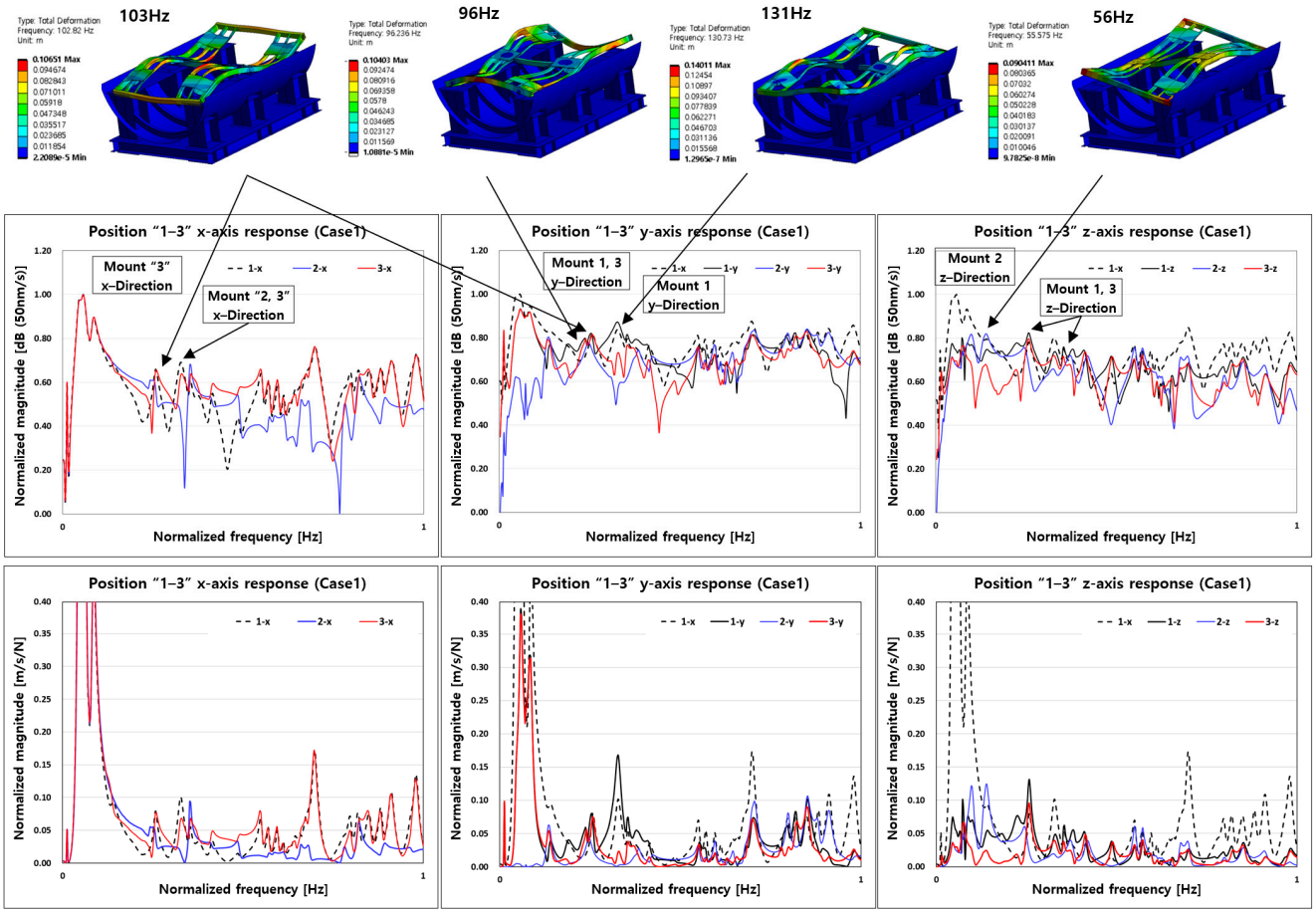

Figure 11. Response at active mount position 1~3 when exciting active mount 1 in the x direction (Case 1).

The results of the vibration mode coupling depending on the stiffness of the middle pedestal are shown in Figure 13, which illustrates that the response characteristics vary significantly with changes in the stiffness of the middle pedestal. Figure 13a presents the vibration response results due to the actuator's control force under Case 1 conditions. In Case 1, it is observed that there are numerous vibration modes associated with the middle pedestal, suggesting that the actuator's control force may induce different vibration modes. This indicates that the system is not independent, and the elements of multiple vibration systems are interacting with each other. Consequently, mode interference occurs due to the control force, and some modes are more dominant, making control at the targeted control frequencies challenging. Additionally, as shown in the phase results on the right side of Figure 13a, the phase varies depending on the position of the 3-axis active mounts, which complicates the calculations for control and is expected to make control more difficult. Figure 13b shows the vibration response results caused by the actuator's control force under Case 2 conditions. As illustrated in this figure, the mode frequencies related to the middle pedestal are shifted backward, resulting in a significantly simplified response and phase characteristics. Fewer vibration modes related to the middle pedestal are present, and the vibration modes are clearly separated, suggesting that control operations will be easier compared to Case 1. Additionally, there are no phase differences among the 3-axis active mount assemblies, which is expected to facilitate control.

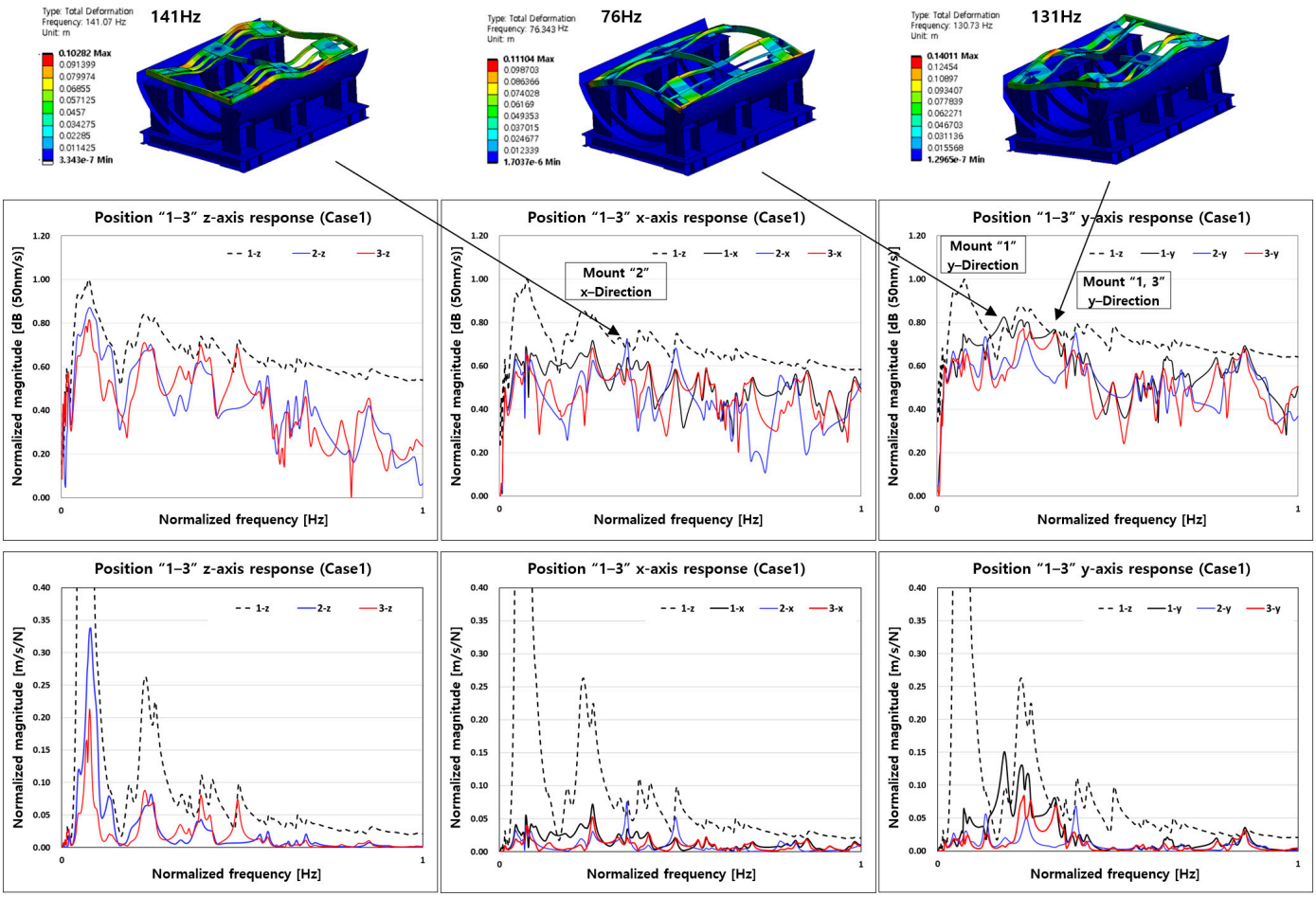

Figure 12. Response at active mount position 1~3 when exciting active mount 1 in the z direction (Case 1).

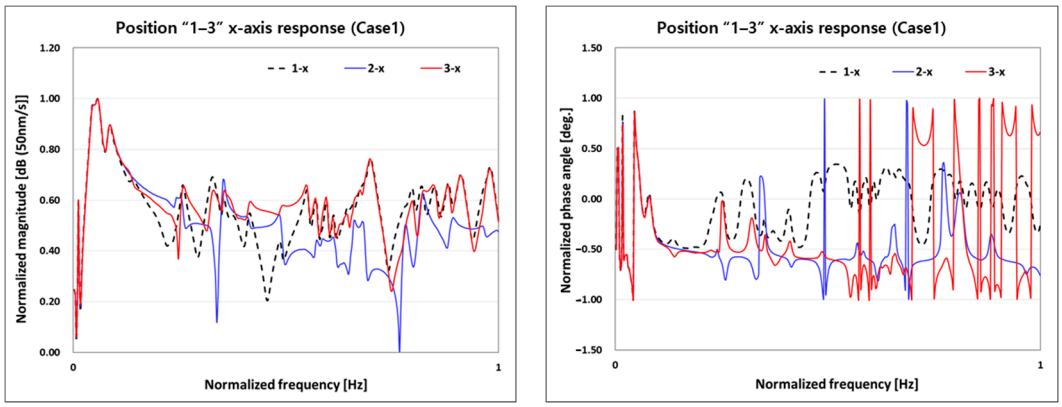

(**a**)

Figure 13. *Cont.*

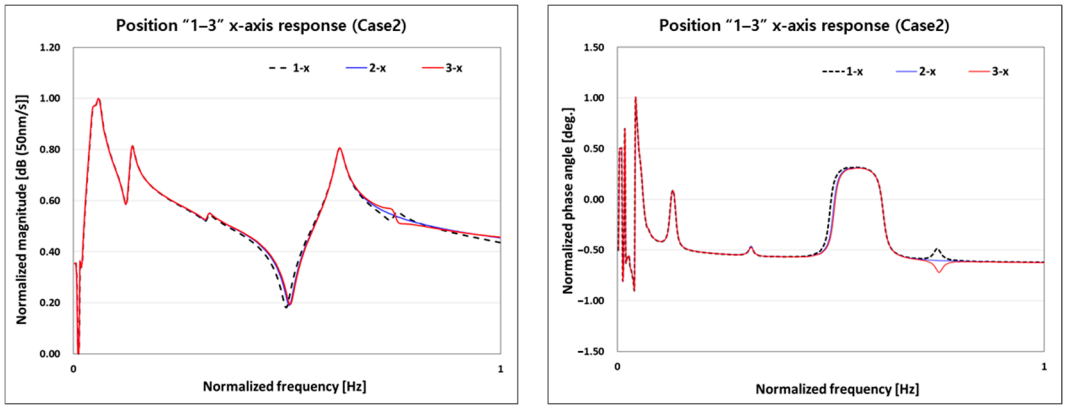

(**b**)

Figure 13. Response at active mount position 1~3 when exciting active mount 1 in the x direction. (**a**) Case 1 (**left**: frequency response, **right**: phase angle), (**b**) Case 2 (**left**: frequency response, **right**: phase angle).

3.2. Active Vibration Control Simulation Result of Ship Vibration Reduction Test Equipment

The control performance based on the stiffness of the middle pedestal was compared using the Fx-LMS algorithm when the excitation force was applied to the mounted equipment. To compare the control performance, vibration control simulations were conducted under identical conditions, and the results were summarized in Table 2. In conclusion, it was predicted that control could be achieved under both Case 1 and Case 2 conditions. However, in Case 1, it took 20 s to achieve the desired vibration reduction performance, whereas in Case 2, control could be achieved within 3 s to meet the target performance. The average vibration reduction amounts for simulations performed under the same conditions are summarized in Table 3. In the model with higher middle pedestal stiffness (Case 2), vibration reduction performance improved, with a minimum of 0.9 dB and a maximum of 13.3 dB.

Table 2. Vibration control success or failure according to the middle pedestal stiffness.

Simulation Condition		Case 1	Case 2
Simulation time [s]	3	x	o
	5	x	o
	10	x	o
	20	o	o

Table 3. Vibration reduction performance according to middle pedestal stiffness [unit: dB, Ref. $5 \times 10-8$ m/s].

Simulation Condition	Case 1			Case 2		
Frequency [Hz]	60 Hz	120 Hz	180 Hz	60 Hz	120 Hz	180 Hz
Average vibration reduction [dB]	22.90	41.19	20.33	24.87	48.43	24.66
	40.62	29.54	14.69	41.47	42.88	23.08
	30.08	41.65	20.07	37.02	44.70	22.05

Figure 14 shows the vibration control results according to the stiffness of the middle pedestal, and it is expected that vibration control is possible under both conditions. In Case 1, mode interference occurs, and a phase difference appears depending on the control location, the three-axis active mount location, but it was confirmed that vibration control is possible by applying control force at different locations. Through this, it was confirmed that control is possible even when the coupling of the system is severe. However, the vibration mode appears differently depending on the control location (mount location), and if the dominant vibration mode is different for each control location, the degree of coupling according to the mode contribution also changes. In this situation, it is natural that the calculation for vibration control becomes very complicated. As can be seen from the results

in Tables 2 and 3 and Figure 14, it takes a relatively long time to complete the control, and unstable control is achieved. In addition, when the control force is applied at a specific mount location, a larger vibration response occurs at another adjacent control location, as can be seen in Figures 11 and 12. This phenomenon occurs because the vibration transmitted from the top and the vibration caused by the control force at the adjacent location overlap, which makes the control operation more complicated. On the other hand, in Case 2, stable control is possible, as can be seen from the vibration control results in Tables 2 and 3 and Figure 14. It can be confirmed that the vibration control is more effective when the vibration mode is clearly separated and the vibration mode and phase according to the control location are very similar. This suggests that it is very important to carefully examine the coupling of the system and select an appropriate stiffness when designing the middle pedestal. When separating the vibration mode and controlling the vibration transmitted from the top, it can be seen that it is important to design the middle pedestal by selecting the stiffness so that additional vibration response does not occur at the adjacent control location.

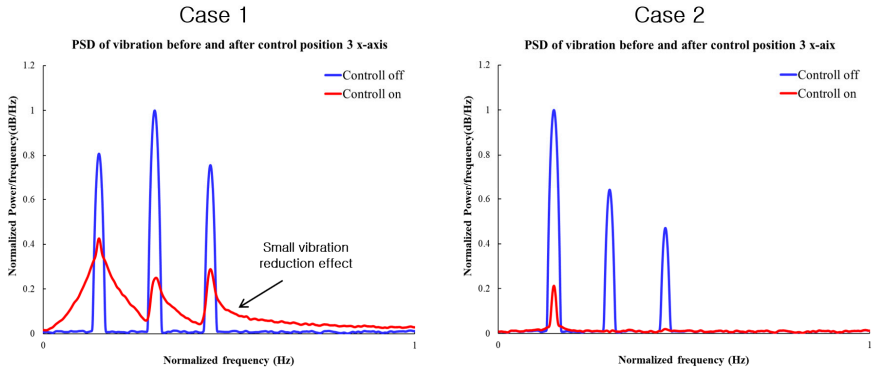

Figure 14. Control results according to the middle pedestal stiffness.

4. Discussion

In this study, the system consisting of the mounted equipment, the three-axis active mount, the middle pedestal, and the mount under the middle pedestal was modeled using finite element analysis (FEA) in a manner similar to the actual mounting conditions. The mobility model was constructed by calculating the frequency response function between the required positions. Using the FEA program, the first path, which is the frequency response function between the excitation force of the mounted equipment and the three-axis active mount at the control position, and the second path, which is the frequency response function between the excitation point of the actuator and the response point of the three-axis active mount at the control position, were obtained. These paths were applied to the vibration control algorithm Fx-LMS, and the vibration control performance was compared based on the stiffness of the middle pedestal. The vibration control simulation confirmed that the control was possible under both Case 1 and Case 2 conditions. However, when the stiffness of the middle pedestal was larger (Case 2), the vibration control was executed faster than in Case 1, and the average range of vibration reduction was 0.9 dB to 13.3 dB, indicating that the vibration reduction performance was improved. The simulation results show that when designing the middle pedestal, it is important to review the coupling of the system to isolate the vibration mode and control the vibration transmitted from the top, and design the middle pedestal with the stiffness selected so that no additional vibration response occurs at the adjacent control location. This simulation model provides a guide for the design of the middle pedestal of a warship and is expected to be useful for preliminary design review before fabricating the middle pedestal in future warship projects.

Author Contributions: Conceptualization, Y.P.; Methodology, Y.P. and K.J.; Analysis, A.J. and K.J.; Simulation, A.J.; Software algorithm, J.H.; Data curation, A.J.; Writing—original draft, A.J.; Supervision, H.L.; Project administration, Hakjun Lee. All authors have read and agreed to the published version of the manuscript.

Funding: This research was supported by the Agency for Defense Development with funding from the government (Defense Acquisition Program Administration) in 2024 (UC210001DD).

Data Availability Statement: The original contributions presented in the study are included in the article, further inquiries can be directed to the corresponding author.

Conflicts of Interest: RMS Technology provided financial support for collaborative research at the authors' institution. However, the funding source had no involvement in the study design, data collection, analysis, interpretation, manuscript preparation, or the decision to publish this paper.

References

1. Park, U.; Lee, J.H.; Kim, K.J. The optimal design of the mounting rubber system for reducing vibration of the air compressor focusing on complex dynamic stiffness. *Mech. Sci. Technol.* **2021**, *35*, 487–493. [CrossRef]
2. Zheng, Y.; Shangguan, W.B.; Yin, Z.; Li, T.; Jiang, J.; Rakheja, S. A hybrid modeling approach for automotive vibration isolation mounts and shock absorbers. *Nonlinear Dyn.* **2023**, *111*, 15911–15932. [CrossRef]
3. Kim, G.; Singh, R. A study of passive and adaptive hydraulic engine mount systems with emphasis on non-linear characteristics. *Sound Vib.* **1995**, *179*, 427–453. [CrossRef]
4. Raoofy, A.; Fakhari, V.; Ohadi, H. Vibration control of an automotive engine using active mounts. *Engine Res.* **2013**, *30*, 3–14.
5. Heinemann, B.; Simanowski, K.; Clasen, M.; Dreesen, J.; Sachau, D. A Testbench for Measuring the Dynamic Force-Displacement Characteristics of Shockmounts. *Vibration* **2024**, *7*, 1–35. [CrossRef]
6. Heinemann, B.; Dreesen, J.; Sachau, D. Dynamic measuring of force-displacement-characteristics of shockmounts. *Heliyon* **2023**, *9*, e16743. [CrossRef] [PubMed]
7. Dario, M.; Massimo, V.; Ignazio, D.; Antonio, C. Active Vibration Control by Piezoceramic Actuators of a Car Floor Panel. In Proceedings of the 23rd International Congress on Sound and Vibration, Athens, Greece, 10–14 July 2016.
8. Dario, M.; Massimo, V.; Monica, C.; Ignazio, D.; Antonio, C. Feasibility study for a tonal vibration control system of a mounting bracket for automotive gearboxes. *Int. J. Mech.* **2016**, *10*, 403–410.
9. Itu, C.; Vlase, S.; Marin, M. A Vibration Analysis of the Rubber Inertial Dampers Used in Electrical Vehicles. *Polymers* **2022**, *14*, 953. [CrossRef] [PubMed]
10. Kauba, M.; Herold, S.; Koch, T.; Mayer, D.; Melz, T. Design and Application of an Active Vibration Control System for a Marine Engine Mount. In Proceedings of the International Conference on Noise and Vibration Engineering, Leuven, Belgium, 15–17 September 2008.
11. Shin, Y.H.; Moon, S.J.; Kwon, J.I.; Jung, W.J.; Jeon, J.J. A new mount with moving-magnet type electromagnetic actuator for naval shipboard equipment. *Nav. Archit. Ocean. Eng.* **2015**, *7*, 41–55. [CrossRef]
12. Moon, S.J.; Choi, S.M.; Nguyen, V.Q.; Oh, J.S.; Choi, S.B.; Chung, J.H.; Kwon, J.I.; Jung, W.J. An inertia-type hybrid mount combining a rubber mount and a piezostack actuator for naval shipboard equipment. *Nav. Archit. Ocean. Eng.* **2013**, *5*, 62–80. [CrossRef]
13. Kim, S.H.; Choi, S.B.; Hong, S.R.; Han, M.S. Vibration control of a flexible structure using a hybrid mount. *Mech. Sci.* **2004**, *46*, 143–157. [CrossRef]
14. López-Romero, M.Á.; Peñas, M.S. A Positive Position Feedback Controller for Vibration Control of Wind Turbines. *Energy Rep.* **2023**, *9*, 1342–1353. [CrossRef]
15. Basten, T.G.H.; Arthur, P.; Vermeulen, R. Active vibration control for underwater signature reduction of a navy ship. In Proceedings of the 17th International Congress on Sound and Vibration, Auburn, AL, USA, 18–22 July 2010.
16. Gupta, A.; Yandamuri, S.; Kuo, S.M. Active vibration control of a structure by implementing filtered-X LMS algorithm. *Noise Contorl Eng.* **2006**, *54*, 396–405. [CrossRef]
17. Yang, D.H.; Shin, J.H.; Lee, H.W.; Kim, S.-K.; Kwak, M.K. Active Vibration Control of Structure by Active Mass Damper and Multi-modal Negative Acceleration Feedback Control Algorithm. *Sound Vib.* **2017**, *392*, 18–30. [CrossRef]
18. Guo, R.; Zhou, Z.; Chen, H. An FxLMS Controller for Active Control Engine Mount with Experimental Secondary Path Identification. *SAE Tech. Pap.* **2020**, *1*, 0424.
19. Kuo, S.M.; Morgan, D.R. Active Noise Control: A Tutorial Review. *Proc. IEEE* **1999**, *87*, 943–973. [CrossRef]
20. Xu, J.; Zhou, W.; Jing, J. An electromagnetic torsion active vibration absorber based on the FxLMS algorithm. *J. Sound Vib.* **2022**, *524*, 116734. [CrossRef]
21. Ll, W.; Wang, W.; Li, B.; Yang, Z. Error Signal Differential Term Feedback Enhanced Variable StepSize FxLMS Algorithm for Piezoelectric Active Vibration Control. *Shock. Vib.* **2020**. [CrossRef]